Chapter

PET Imaging of Mitochondrial Function in the Living Brain

Hideo Tsukada

Abstract

In the last two and half decades, we have conducted research on brain functional imaging in nonhuman primates using animal positron emission tomography (PET) scanners with high spatial resolution. We recently designed and synthesized the novel PET probe [^{18}F]BCPP-EF to quantitatively image mitochondria complex-I (MC-I) activity in the living brain. Brain MC-I activity, measured using [^{18}F] BCPP-EF, was significantly lower in aged monkeys than that in young animals, while no significant reduction was observed in SV2A activity, a synaptic-specific parameter that was measured using [^{11}C]UCB-J. Some aged monkeys exhibited increased amyloid-β deposition in the brain, measured using [^{11}C]PiB, which induced neuroinflammation. A positive correlation was noted with neuroinflammation, measured using [^{11}C]DPA-713 and a negative correlation with MC-I activity. Furthermore, a monkey model of Parkinson's disease prepared by the chronic administration of MPTP revealed suppressed MC-I activity not only in the nigrostriatal dopamine pathway, measured using [^{11}C]PE2I and [^{11}C]6Me*m*Tyr, but also in cortical serotonergic neurons, measured using [^{11}C]DASB. This review introduces the translational application of a novel PET probe for noninvasive MC-I imaging from preclinical to clinical PET measurements.

Keywords: brain, mitochondria, aging, neurodegeneration, PET

1. Introduction

The brain has the most complex system among all human organs and plays a central role in physiological, neurological, and metabolic regulation throughout the body. The brain is very metabolically active in proportion to its volume, consuming 20% of total oxygen and 25% of total glucose, and each cell relies on mitochondria to produce energy as adenosine triphosphate (ATP). The brain consists of neuronal and glial cells, each of which uses the different metabolic pathways to produce ATP; astrocytes are highly glycolytic, while neurons depend on oxidative phosphorylation (OXPHOS) in the mitochondria [1]. The electron transport chain (ETC) for OXPHOS in mitochondria consists of five types of complexes from I to V, with complex-I (MC-I; NADH–ubiquinone oxidoreductase, EC 1.6.5.3) forming the first and rate-limiting steps of overall respiratory and OXPHOS.

Neuronal death is regarded the dominant cause of brain aging. The "Mitochondrial Free Radical Theory of Aging" considers mitochondria to be the main drivers of aging due to the generation of reactive oxygen (ROS) and nitrogen (RNS) species through the ETC, and the cumulated impairment of mitochondria by oxidative stress in mitochondrial lipids, proteins, and DNA leads to neuronal

death in the brain [2]. Neuronal damage related to impaired mitochondrial function is a hallmark for several neurodegenerative diseases, including Alzheimer's (AD), Parkinson's (PD), Huntington's diseases (HD), as well as amyotrophic lateral sclerosis (ALS) and multiple sclerosis (MS).

The etiology of AD, the most prominent age-related neurodegenerative disease, is multifactorial and associated with various environmental and genetic factors that play a role in its pathogenesis. The deposition of amyloid-β (Aβ) in the brain has been suggested to enhance neurodegenerative damage. Structural disruption and loss of neuronal cells induced by Aβ, leading to neuronal network dysfunction and synaptic loss in the hippocampus and cerebral cortex, is associated with cognitive impairment in AD patient [3]. Although the molecular mechanisms underlying synaptic dysfunction induced by Aβ have not been fully elucidated, mitochondrial dysfunction caused by Aβ is associated with synaptic functional alterations in the living brain [3].

PD is the second most prominent neurodegenerative disease and is characterized by the progressive degradation of the nigrostriatal pathway with the selective loss of dopamine (DA) neurons, resulting in movement abnormalities such as resting tremor, rigidity, akinesia, and impaired postural reflexes. A hallmark of idiopathic PD is the deposition of Lewy bodies containing insoluble and aggregated α-synuclein in the cytoplasmic fraction of nigrostriatal neurons in the DA pathway [4]. The loss of MC-I catalytic activity in the ETC has been reported in tissues obtained from sporadic PD patients [5] with increased oxidative stress [6].

Regarding the noninvasive assessment of mitochondrial function in the living brain, we recently developed a novel probe, [^{18}F]2-tert-nutyl-4-chloro-5-{6-[2-(2-fluoroethyl)-ethoxyl-pyridin-3-3-ylmetoxy]-2H-pyrisazin-3-one ([^{18}F]BCPP-EF), for positron emission tomography (PET) [7]. The effects of physiological aging, aging-related Aβ deposition, and chronic MPTP treatments on cortical MC-I function were assessed in conscious monkeys using [^{18}F]BCPP-EF, with the aim of translating clinical PET research to AD and PD patients.

2. Effects of aging on MC-I and SV2A function in the living brain

Mitochondria from aged brains consume less oxygen and, thus, produce lower amounts of ATP [8]. Different types of neurons show differences in topologies with various numbers of synaptic connections. Since synaptic and non-synaptic mitochondria have different protein compositions and respiratory and ROS production rates, synaptic mitochondria are more vulnerable to oxidative damage during the aging process than non-synaptic mitochondria [9]. In quantitative assessments of the effects of physiological aging on mitochondria and synaptic function in the living brain, the activities of MC-I and synaptic vesicle glycoprotein 2A (SV2A), an ideal biomarker for synaptic density, were comparatively evaluated in the living brains of young and aged rhesus monkeys.

2.1 Methods

Six young male (3–5 years old) and eight aged male (20–24 years old) rhesus monkeys (*Macaca mulatta*) were examined in the PET study using [^{18}F]BCPP-EF for MC-I and (*R*)-1-((3-[^{11}C]methyl-[^{11}C])pyridine-4-yl)methyl)-4-(3,4,5-trifluorophenyl)pyrrolidin-2-one ([^{11}C]UCB-J) for SV2A [10]. MRI was performed on each monkey using a 3.0 T MR imager (Singna Excite HDxt 3.0 T, GE Healthcare) using a 3D spoiled gradient echo (SPGR) sequence under pentobarbital anesthesia. To avoid anesthetic effects on brain function as well as PET probe kinetics, PET scans were

conducted under conscious condition using high-resolution animal PET scanners (SHR-7700 and 38,000, Hamamatsu Photonics) as reported previously [11–14].

[^{18}F]BCPP-EF was prepared by the nucleophilic [^{18}F] fluorination of the corresponding precursor, as reported previously [9]. Radiochemical purity was more than 99%, and specific radioactivity was 47.8 ± 12.7 GBq/μmol. [^{11}C]UCB-J was labeled via the Suzuki cross-coupling of [^{11}C]methyl iodide with a boronate precursor, as reported previously [10]. Radiochemical purity was more than 98%, and specific radioactivity was 62.3 ± 25.1 GBq/μmol.

After overnight fast, a venous cannula for the PET ligand injection and an arterial cannula for blood sampling were inserted into both inferior limbs. The animal's head was rigidly fixed to a monkey chair using an acrylic head-restraining device surgically attached on the skull. The monkey sitting in the chair was placed at a position in the PET gantry with stereotactic coordinates aligned parallel to the orbito-metal (OM) plane. After a transmission scan for 30 min using a [^{68}Ge]-[^{68}Ga] rotation rod source, a dynamic emission scan with [^{18}F]BCPP-EF or [^{11}C] UCB-J was conducted for 90 min after the PET probe injection as a bolus.

To assess the specificity of [^{18}F]BCPP-EF binding to MC-I, which was previously examined in rats [15], rotenone, an MC-I inhibitor, at a dose of 0.1 mg/kg was infused into young monkeys through a vein cannula for 1 h, followed by [^{18}F] BCPP-EF injection.

PET data were reconstructed by the dynamic row action maximum likelihood algorithm (DRAMA) method using a 2.0-mm Gaussian post filter [16], with attenuation correction using transmission scan data. Individual PET and MRI images were co-registered. Volumes of interest (VOIs) in brain regions were drawn manually on MRI, and the time activity curve (TAC) of each PET probe was taken for kinetic analyses. These imaging annalistic processes were performed using PMOD software (PMOD Technologies Ltd.).

In a quantitative analyses of [^{18}F]BCPP-EF and [^{11}C]UCB-J, arterial blood samples were frequently obtain after the PET probe injection, centrifuged to separate plasma, and ethanol was added to some plasma samples, followed by centrifugation. The supernatants obtained were developed with thin layer chromatography with a mobile phase of ethyl acetate for [^{18}F]BCPP-EF and chloroform/methanol = 9:1 for [^{11}C]UCB-J, respectively. The ratio of the unmetabolized fraction was assessed using a phosphoimaging plate analyzed by a bioimaging analyzer (FLA-7000, GE Healthcare).The arterial input function of unmetabolized [^{18}F]BCPP-EF or [^{11}C]UCB-J was calculated using data obtained by a correction of the radioactivity ratio in the unmetabolized fraction to total fraction. A kinetic analysis of [^{18}F] BCPP-EF or [^{11}C]UCB-J was performed to calculate distribution volume (V_T) using a Logan graphical analysis [17] with PMOD software (PMOD Technologies Ltd.).

2.2 Results

Brain TACs of [^{18}F]BCPP-EF in young animals peaked at approximately 15 min after the injection, except in the occipital cortex, which peaked at 40 min, and TACs then were gradually eliminated with time under conscious condition. The pre-administration of rotenone resulted in a faster elimination rate of [^{18}F]BCPP-EF from the brain than that in normal. In aged animals, the peak time of TACs shifted to slightly later after the injection and showed significant lower [^{18}F]BCPP-EF uptake levels than those in young animals.

The washout of [^{18}F]BCPP-EF-related radioactivity and its metabolites rate in plasma were very rapid, with only 10% of the non-metabolized parent probe remaining 60 min after the injection. These kinetic patterns of [^{18}F]BCPP-EF were almost identical among control young, rotenone-treated young, and aged animals.

A metabolic analysis confirmed that its metabolites were very polar, indicating no uptake of metabolites into the brain through the blood–brain barrier. These results confirmed that this PET probe has ideal properties for the quantitative analysis of MC-I activity using a metabolite-corrected arterial input function.

As shown in the upper panel of **Figure 1**, V_T-PET images of young brains indicated that the binding of [^{18}F]BCPP-EF was highest in the occipital cortex, higher in the striatum, intermediate in the frontal and temporal cortices and cerebellum, and lowest in the hippocampus. The pre-administration of rotenone at a dose of 0.1 mg/kg/h significantly reduced the uptake of [^{18}F]BCPP-EF into the young monkey brain, specifically in the frontal and temporal cortices and striatum. When aging effects on V_T-PET images were assessed, the binding of [^{18}F]BCPP-EF throughout the brain was significantly lowered in aged animals than in young animals, as shown in the lower panel of **Figure 1**.

The TAC of [^{11}C]UCB-J in young animals exhibited slower kinetics than [^{18}F]BCPP-EF throughout the brain regions, peaking approximately 30 min after the injection, and TACs gradually decreased with time under conscious conditions. TACs in aged animals peaked 30 min after the injection and showed slightly lower [^{11}C]UCB-J uptake levels than those in young animals. The washout of [^{11}C]UCB-J-related radioactivity and metabolic rates in plasma were slower than those of [^{18}F]BCPP-EF, with 25% of the non-metabolized parent probe remaining 60 min after the injection. These kinetic patterns of [^{18}F]BCPP-EF were not significantly different between young and aged animals. A metabolic analysis confirmed that its metabolites were very polar, suggesting no uptake of the metabolites into the brain through the blood–brain barrier. These results confirmed that this PET probe is useful for the quantitative analysis of SV2A activity using a metabolite-corrected arterial input function.

As shown in the upper panel of **Figure 2**, V_T-PET images of the young brain revealed the highest binding of [^{11}C]UCB-J in the frontal, temporal, and occipital

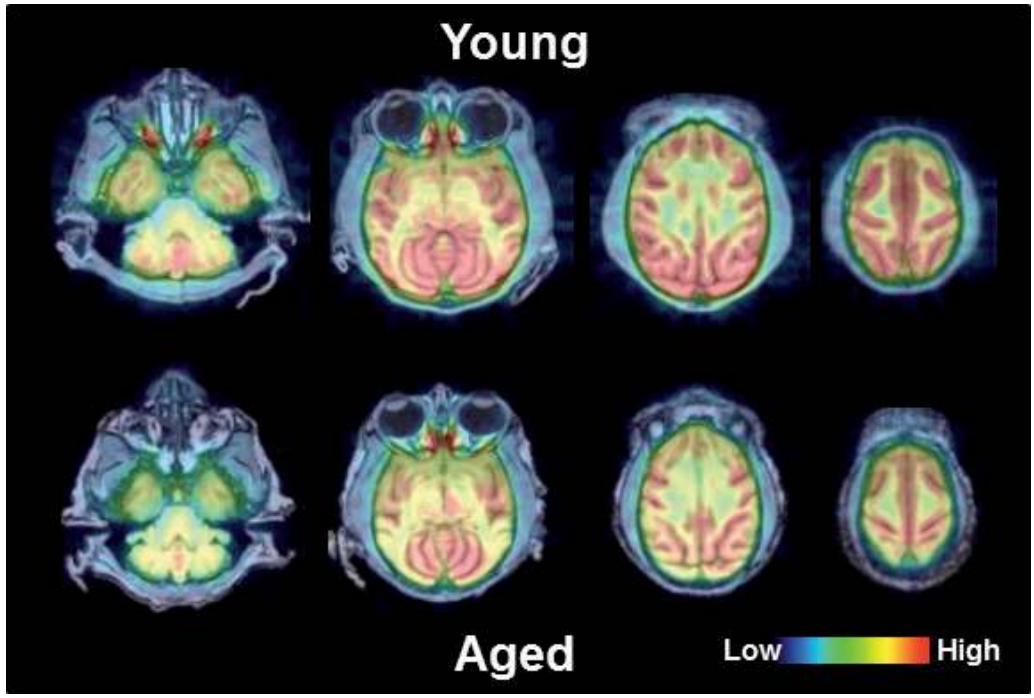

Figure 1.
Effects of aging on PET images of MC-I in living brains of conscious monkeys. PET scans were conducted for 91 min using [^{18}F]BCPP-EF for MC-I, and V_T images of [^{18}F]BCPP-EF were created using a Logan graphical plot analysis with metabolite-corrected plasma input.

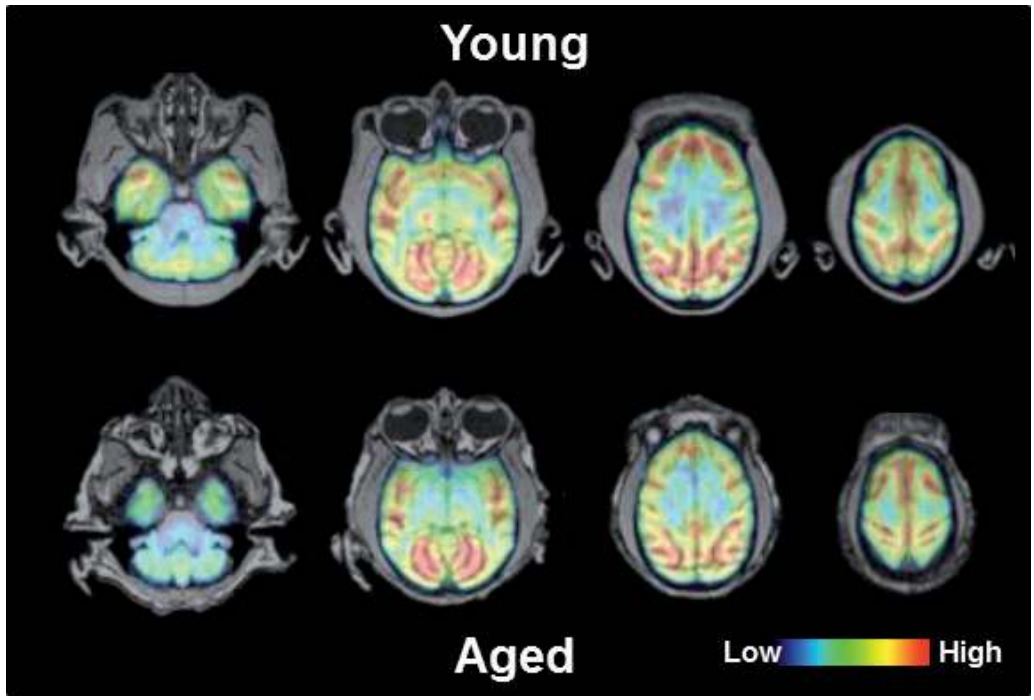

Figure 2.
Effects of aging on PET images of SV2A in living brains of conscious monkeys. PET scans were conducted for 91 min using [^{11}C]UCB-J for SV2A, and V_T images of [^{11}C]UCB-J were created using a Logan graphical plot analysis with metabolite-corrected plasma input.

cortices, higher in the striatum, intermediate in the hippocampus, and the lowest in the cerebellum. Thus, the distribution pattern of [^{11}C]UCB-J resembled to that of [^{18}F]BCPP-EF throughout the brain of young animal.

However, in contrast to [^{18}F]BCPP-EF, when the V_T of [^{11}C]UCB-J was compared between young and aged monkeys, no significant age-related changes in cerebral SV2A activity were detected except the olfactory bulb, as shown in the lower panel of **Figure 2**.

2.3 Discussion

The present results showed age-related reduction in mitochondria function assessed by MC-I activity using [^{18}F]BCPP-EF, as reported previously [11], while no significant alterations in synaptic density were observed based on SV2A activity using [^{11}C]UCB-J.

We evaluated [^{18}F]BCPP-EF by in vitro (living brain slices), ex vivo (dissected tissues), and in vivo (living rat brains) assessments in comparison with the conventional MC-I PET probe, [^{18}F]BMS-747158-02 ([^{18}F]BMS), which was developed as a myocardial perfusion PET imaging probe [18], and the results obtained suggested that [^{18}F]BCPP-EF is a more suitable PET probe than [^{18}F]BMS for MCI assessments in the living brain [7, 15]. [^{18}F]BCPP-EF was characterized by (1) high specific binding with moderate affinity, (2) a proper log$D_{7.4}$ value, (3) long metabolic stability with fast clearance in plasma, (4) sufficient brain uptake with a proper elimination rate from the brain, and (5) low dependency to cerebral blood flow changes [19]. As a PET probe, these properties of [^{18}F]BCPP-EF may contribute for a noninvasive and quantitative analysis of MC-I in the living brain [11], thereby allowing for the high detectability of age-related reductions in MC-I activity in the living monkey brain. Although several postmortem in vitro studies previously reported that (1)

age-related brain MC-I impairments were associated with a decline in mitochondria respiration [20, 21] and (2) the activities of MC-I and -IV, but not MC-II, III, or V, decreased with aging in the brains of rodents [22] and humans [20, 21], this study was the first to successfully confirm age-related reductions in MC-I activity in the living brain of nonhuman primates [11].

As described above, [^{18}F]BCPP-EF detected age-related reduction in MC-I activity; however, this PET probe was unable to discriminate the subdomain (synapse, dendrites, or soma) of MC-I that was exclusively damaged due to the limitation of the spatial resolution of PET. In attempts to answer this question, [^{11}C]UCB-J, a novel PET probe for SV2A [10], was applied to the same subject groups on the assumption that if this MC-I reduction mainly reflected the presynaptic domain, the binding of [^{11}C]UCB-J to SV2A will also show a similar age-related reduction pattern in the brain. However, contrary to this assumption, no significant changes in [^{11}C]UCB-J binding to SV2A were observed, except the olfactory bulb, from those in the same young and aged animals applied in the assessment using [^{18}F]BCPP-EF.

Several postmortem in vitro studies have suggested age-related reductions in spine density; however, these findings remain controversial. One study using rat brains revealed that the synaptic vesicle density in axospinous synapse, a major population of synapses, rapidly increased until 3 weeks old and then decreased to the adult level, followed by no changes in senescence [23]. However, another study on mouse brain showed that age-related deficits in sensory perception were not associated with synaptic loss in the somatosensory cortex but were related to alterations in the size and stability of spine buttons [24], which might not be detected as the changes in SV2A activity.

The discrepancy in age-related effects between [^{11}C]UCB-J and [^{18}F]BCPP-EF suggest that MC-I dysfunction detected by [^{18}F]BCPP-EF mainly reflect neuronal damage in dendrite and soma domains and are not specific to presynaptic domain. Although difficulties are associated with assessing mitochondrial distribution in neuronal cells, it was demonstrated in the cultured neuron that more than 90% of mitochondria were confirmed to be in the dendrite shaft overlapping in soma and large-diameter proximal dendrites [25]. This localized distribution pattern of the mitochondria suggests that even if mitochondria in the presynaptic domain are specifically impaired, difficulties may be associated with detecting changes in the minor subdomain using [^{18}F]BCPP-EF. The present results also suggested that in the early stage of the aging process, at least, in nonhuman primates, neuronal damage in the synaptic domain, if any, may be too subtle to be detected as decreased [^{11}C]UCB-J binding to SV2A.

3. Effects of amyloid-β deposition on MC-I function in the living brain

Patients of AD, the most prominent age-related neurodegenerative disease, are characterized by the deposition of fibrillary Aβ into senile plaques and hyperphosphorylated tau (P-tau) into neurofibrillary tangle (NFT) in the brain. Monomer Aβ has been implicated in normal developmental synaptic plasticity, for example, in the olfactory bulb under physiological conditions [26]. However, the aggregation of Aβ switches its physiological role into a pathologically toxic function; thus dense plaques damage the surrounding brain tissues [27], causing synaptic elimination and impaired synaptic function [28]. Although the molecular mechanisms underlying neuronal damage induced by Aβ have not been fully elucidated, mitochondrial dysfunction may be associated with Aβ-induced synaptic dysfunction [3] and also with neuroinflammation [29], resulting in cognitive impairment in AD patients. In order to clarify the relationship between Aβ deposition, neuroinflammation, and mitochondrial function, [^{11}C]PiB for Aβ [30], [^{11}C]DPA-713 for translocator protein

(TSPO) [31], and [^{18}F]BCPP-EF for MC-I were comparatively evaluated in the living brains of aged rhesus monkeys. Furthermore, as a gold standard parameter of cerebral metabolism, [^{18}F]fluoro-2-deoxy-D-glucose ([^{18}F]FDG) was also applied to compare the diagnostic and prognostic usefulness with [^{18}F]BCPP-EF.

3.1 Methods

Twenty aged male (20–24 years old) rhesus monkeys (*Macaca mulatta*) were investigated in the PET study using [^{11}C]PiB for Aβ, [^{11}C]DPA-713 for TSPO, and [^{18}F]BCPP-EF for MC-I under conscious conditions using a high-resolution PET scanner as described in 2.1.

[^{11}C]PiB was synthesized by the *N*-methylation of nor-compound *N*-desmethyl-PiB with [^{11}C]methyl triflate [30]. Radiochemical purity was more than 99%, and specific radioactivity was 36.7 ± 10.1 GBq/μmol. [^{11}C]DPA-713 was synthesized by the *N*-methylation of nor-compound *N*-desmethyl-DPA with [^{11}C] methyl triflate [31]. Radiochemical purity was more than 99%, and specific radioactivity was 99.3 ± 32.2 GBq/μmol. [^{18}F]BCPP-EF was radiolabeled as shown in 2.1. Radiochemical purity was more than 99%, and specific radioactivity was 139.6 ± 37.0 GBq/μmol. [^{18}F]FDG was produced by the nucleophilic [^{18}F]fluorination of mannose triflate following the basic hydrolysis of 2-[^{18}F] fluoro-1.3.4.6-tetra-*O*-acetyl-D-glucose.

In the analysis of [^{11}C]PiB, standard uptake value (SUV) images from 60 to 90 min were created, VOIs were set on each SUV images, and the SUV ratios (SUVR) of each region (SUVreg) against SUV in the cerebellum (SUVcereb) were calculated [32]. In the analysis of [^{11}C]DPA-713, SUV images from 40 to 60 min were created, and VOIs were set on each SUV image. Since any cerebral regions were not applicable as the reference region with negligible TSPO levels [33], the SUV, not SUVR, was assessed. A quantitative analysis of [^{18}F]BCPP-EF was performed as described in 2.1. During PET scanning with [^{18}F]FDG, continuous arterial sampling was conducted, and PET images from 40 to 60 min after the injection were obtained to calculate the regional cerebral metabolic rate of glucose (rCMRglc) using an autoradiographic method. The rCMRglc ratios of each region (rCMRglc-region) against rCMRglc in the cerebellum (rCMRglc-cere) were calculated [34].

3.2 Results

Since the cortical V_T values of [^{18}F]BCPP-EF in aged monkeys were previously shown to have a higher CV value of ca. 25% than those in young ones of ca. 7% [11], the reasons for the lager variation of MC-I activity were elucidated using PET imaging with [^{11}C]PiB for Aβ deposition and [^{11}C]DPA-713 for TSPO in 20 aged monkeys. **Figure 3** shows the PET/MRI images of aged monkeys with the lowest (A) and highest (E) [^{11}C]PiB binding, with high SUV not only being detected in cortical but also subcortical regions. PET results obtained with [^{11}C]PiB were supported by an immunohistochemical assessment conducted after PET assessments [12]. The images of [^{11}C]DPA-713 (B and F) corresponding to each monkey (A and E) revealed that monkeys with the lowest (A) and highest (E) [^{11}C]PiB binding showed the lower (B) and higher (F) [^{11}C]DPA-713 binding. In contrast, the images of [^{18}F] BCPP-EF corresponding to each monkey with the lowest (A) [^{11}C]PiB binding exhibited higher [^{18}F]BCPP-EF uptake (C), while those with the highest [^{11}C]PiB binding (E) showed the lower [^{18}F]BCPP-EF uptake (G).

As shown in **Figure 4A**, when the SUV values of [^{11}C]DPA-713 were plotted against the SUVR of [^{11}C]PiB in the cortical VOIs of all animals, the results obtained revealed a significant positive correlation between each parameter,

indicating that Aβ deposition-induced neuroinflammation in the living brains of aged monkeys. In contrast, the plotting of V_T of [^{18}F]BCPP-EF against SUVR of [^{11}C]PiB showed a reverse correlation in the cortical VOIs of all animals, suggesting that Aβ deposition-induced MC-I impairments in the brains of aged monkeys (**Figure 4B**).

Based on **Figures 3H** and **4C**, it is important to note that a correlation was not observed between glucose metabolism assessed as the SUVR of [^{18}F]FDG and Aβ deposition measured as the SUVR of [^{11}C]PiB, and this may have been due to [^{18}F]FDG uptake into the neuroinflammation-related activated microglial cells.

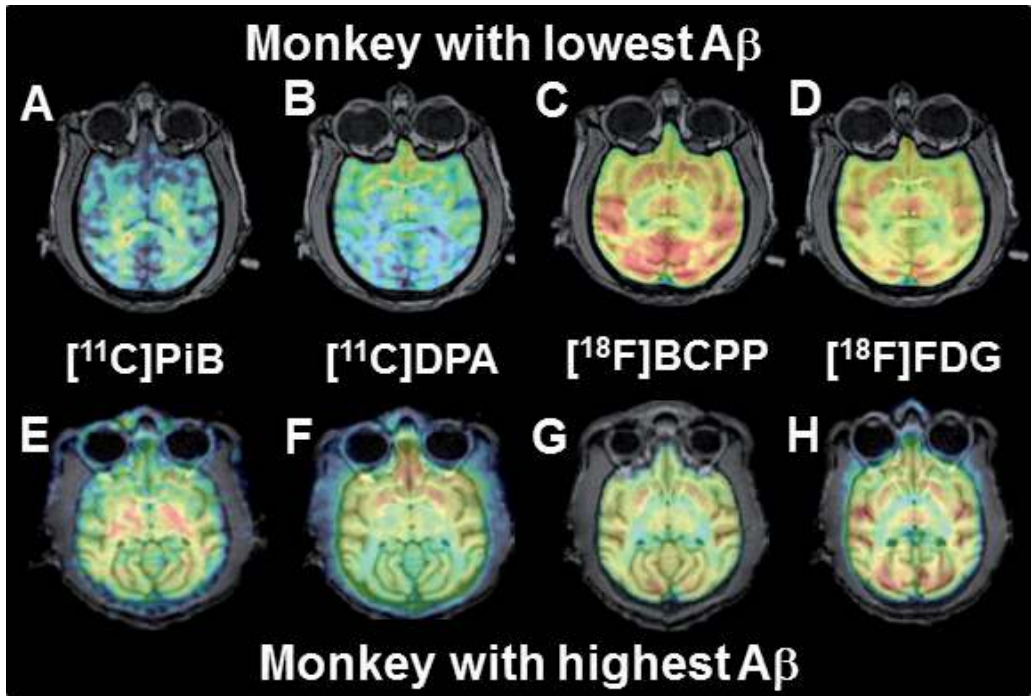

Figure 3.
Effects of Aβ deposition on PET images of [^{11}C]PiB (A and E), [^{11}C]DPA-713 (B and F), [^{18}F]BCPP-EF (C and G), and [^{18}F]FDG (D and H) in living brains of conscious monkeys. PET scans were conducted in monkey with the lowest (A–D) and highest (E-H) Aβ deposition among 20 aged monkeys.

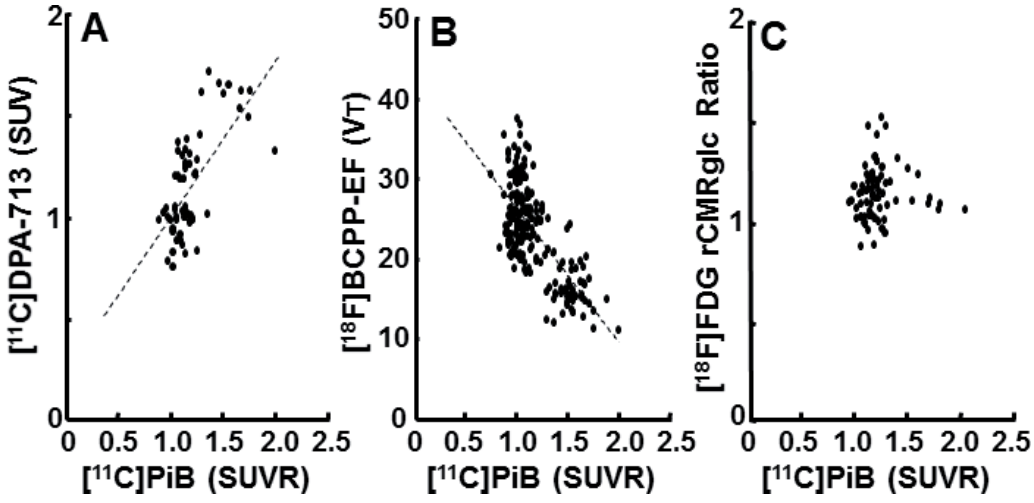

Figure 4.
Correlations between the SUV of [^{11}C]DPA-713 (A), V_T of [^{18}F]BCPP-EF (B), and rCMRglc ratio of [^{18}F]FDG (C) against the SUVR of [^{11}C]PiB in cortical and hippocampal regions of living brains of aged monkeys.

3.3 Discussion

The present results demonstrated the potential of MC-I impairment assessed using [^{18}F]BCPP-EF as a useful biomarker for Aβ deposition-related neurodegeneration, measured using [^{11}C]PiB, and neuroinflammation, measured using [^{11}C]DPA-713. In contrast, the assessment of rCMRglc using conventional [^{18}F]FDG was not as sensitive for detecting the neurodegenerative damage associated with inflammation in the early stage of disease onset because of [^{18}F]FDG uptake into not only normal neuronal cells but also into inflammatory cells, such as activated microglia in the brain [15, 19, 29]. Since activated microglia dominantly facilitate glycolysis, not ORPHOS system through mitochondria, to produce ATP, more glucose is required in microglia than in normal neuron, resulting in higher [^{18}F]FDG uptake than in normal cells. Thus, MC-I assessed using [^{18}F]BCPP-EF has a potential as a biomarker to assess neurodegeneration more accurately without being affected by inflammation in the living brain.

The present PET images obtained using [^{11}C]PiB did not reveal as prominent Aβ deposition in aged monkey brains as that in the brains of PD patients. Previous studies suggested that no species other than humans exhibited marked neuron loss or cognitive impairment observed as clinical grade AD in humans, and aged monkeys did not exhibit as high Aβ deposition as seen in AD patients [35] or [^{11}C]PiB binding [36] as that in AD patients. Therefore, we assumed that the aged monkey model exhibited a similar mild cognitive impairment (MCI)-like, not AD-like, state to that in humans. In the AD state after a lag period of MCI, Aβ deposition level reached a plateau; therefore no correlation was observed between [^{11}C]PiB uptake and cognitive levels or metabolic dysfunction assessed using [^{18}F]FDG [37]. In contrast, [^{11}C]PiB may function as a quantitative and sensitive biomarker for Aβ-related neuronal damage in aged monkey brains resembling the MCI-like state in humans [38]. Furthermore, a recent study reported the primary role of non-deposited, non-fibrillar assembles of Aβ peptides, and, thus, they may become precursors for fibrillogenesis, which lead to oxidative neurotoxicity by ROS in the brains of very early stage of AD patients [39]. ROS-related mitochondrial OXPHOS failure in the brain has been implicated in neurodegenerative disorders [40]. Mitochondria are the main intercellular source of ROS and also the main target of oxidative damage, leading to the significant disruption of brain function. A recent study demonstrated the direct effects of Aβ on mitochondria; thus, in addition to extracellular deposition, Aβ was detected in cytoplasmic mitochondria compartments [41], leading to dysfunction with the suppressed availability of nucleus-encoded proteins, a decreased rate of NABH reduction, and enhanced ROS generation [42]. Since we previously confirmed a positive correlation between the V_T of [^{18}F]BCPP-EF and $rCMRO_2$, a gold standard for brain activation [19], the Aβ deposition-related MC-I functional impairment observed in the present study may reflect diminished activity and/or the loss of neurons with neuroinflammation. The present study revealed a correlation between [^{11}C]PiB binding and [^{18}F]BCPP-EF uptake, demonstrating the usefulness of an assessment of MC-I for the diagnostic staging of MCI and early stage AD.

In the present study, TSPO activity evaluated using [^{11}C]DPA-713, an index of neuroinflammation, was stronger in the aged monkey brain with higher [^{11}C]PiB binding to Aβ. Furthermore, [^{11}C]DPA-713 binding to TSPO and rCMRglc measured using [^{18}F]FDG revealed a correlation (data not shown) [12]. These results suggest Aβ deposition-induced neuroinflammation with the activation of microglial cells.

Therefore, the detectability of MC-I impairment using [^{18}F]BCPP-EF for neuronal damage in AD appears to be superior to the assessment of glucose metabolism measured using conventional [^{18}F]FDG.

4. Effects of MPTP-induced parkinsonism on MC-I in the living brain

Patients with PD show the progressive degradation of the nigrostriatal pathway with the selective loss of DA neurons in the substantia nigra pars compacta (SNc), resulting in movement disorders, which are induced after the loss of ca. 50% of neurons in the SNc and a reduction in DA to ca. 20% of normal levels in the striatum [43]. A pathological hallmark of PD is Lewy bodies and Lewy neurites, containing intracytoplasmic insoluble and aggregated protein of α-synuclein [4]. The spread of these pathologies closely correlates with disease progression. Furthermore, an intracerebral injection of insoluble α-synuclein converted normal α-synuclein into an abnormal form, which then propagated throughout the brains of monkeys [44] and common marmosets [45]. The soluble, β sheet-rich oligomers of α-synuclein induced mitochondrial dysfunction by inhibiting MC-I, enhancing ROS production, and activating the mitochondrial permeability transition pore (PTP), leading to mitochondrial swelling and neuronal death [46].

Since exposure to 1-methyl-4-phenyl-1,2,3,6-tetrahydropyridine (MPTP) induces a syndrome mimicking PD symptoms accompanied by selective DA damage in the nigrostriatal pathway [47], we developed a PD model of monkeys by systemic and repeated MPTP administration [48, 49] and evaluated serotonin (5-HT) transporter (SERT) availability using [^{11}C]-3-amino-4-(2-dimethylaminomethylphenylsulfanyl)-benzonitrile ([^{11}C]DASB) [50] 5-HT 1A receptor (5-HT$_{1A}$R) binding using 4-(2′-methoxyphenyl)-1-[2′-(*N*-2″-pyridinyl)-*p*-[^{18}F]fluoro-benzamido]ethylpiperazine ([^{18}F]MPPF) [51] in parallel with DA parameters for presynaptic DA synthesis (DAS) using 6-[^{11}C]methyl-*m*-tyrosine ([^{11}C]6Me*m*Tyr) [52, 53], DA transporter (DAT) using [^{11}C]*N*-(3-iodoprop-2E-enyl)-2β-carbomethoxy-3β-(4-methyl-phenyl) nortropane ([^{11}C]PE2I) [54], postsynaptic DA D$_2$R using [^{11}C]Raclopride, and MC-I activity using [^{18}F]BCPP-EF in the living brains of MPTP-treated monkeys [13].

4.1 Methods

Young adult male rhesus monkeys (*Macaca mulatta*) were used to prepare the PD model, as reported previously [48, 49]. MPTP at doses ranging between 0.2 and 0.4 mg/kg in phosphate-buffered saline was injected intravenously over a 4-month period until stable Parkinsonian syndrome developed. MPTP-treated monkeys were subjected to PET scans using specific PET probes for DA, 5-HT neuronal systems, and MC-I under conscious condition using a high-resolution PET scanner, as described in 2.1. In order to avoid the potential for spontaneous recovery as well as direct inhibition of [^{18}F]BCPP-EF binding to MC-I by MPTP, all PET measurements were started at least after 2 months after the last treatment with MPTP.

[^{11}C]PE2I was radiolabeled by the *O*-[^{11}C]methylation of its nor-compound with [^{11}C]methyl triflate. Radiochemical purity was more than 98% and specific radioactivity of 117.1 ± 42.9 GBq/μmol. [^{11}C]6Me*m*Tyr was developed in our laboratory using rapid Pd(0)-mediated cross-coupling between [^{11}C]methyl iodide and its boronate precursor [52, 53], showing radiochemical purity of more than 99% and specific radioactivity of 71.6 ± 37.4 GBq/μmol. [^{11}C]Raclopride was radiolabeled by *N*-[^{11}C]methylation of its nor-compound with [^{11}C]methyl triflate. Radiochemical purity was more than 98% and specific radioactivity of 65.4 ± 15.8 GBq/μmol. [^{18}F]BCPP-EF was radiolabeled as shown in 2.1. Radiochemical purity was more than 99%, and specific radioactivity was 58.9 ± 7.9 GBq/μmol. [^{11}C]DASB was prepared by the *N*-[^{11}C]methylation of its nor-compound with [^{11}C]methyl triflate [50] with radiochemical purity of more than 99% and specific radioactivity of

47.6 ± 11.1 GBq/μmol. [^{18}F]MPPF was synthesized by the nucleophilic [^{18}F]fluorination of its nitro precursor [51] with radiochemical purity of more than 99% and specific radioactivity of 90.4 ± 25.6 GBq/μmol.

Quantitative analyses of [^{11}C]PE2I, [^{11}C]Raclopride, [^{11}C]DASB, and [^{18}F]MPPF were performed with a simplified reference tissue model to calculate non-displaceable binding potential (BP_{ND}) [55] using PMOD software (PMOD Technologies Ltd., Zurich, Switzerland). As an indirect input function, TAC in the cerebellum was applied. A quantitative analysis of [^{18}F]BCPP-EF was performed as described in 2.1. A quantitative analysis of [^{11}C]6Me*m*Tyr to calculate the Ki value was performed using a multiple-time graphical analysis [56] using PMOD software (PMOD Technologies Ltd., Zurich, Switzerland) applying the TAC in the occipital cortex as an input function.

4.2 Results

The effects of chronic MPTP treatments on the DA neuronal system in the brain were revealed in **Figure 5**. PET measurements using [^{11}C]PE2I for DAT (A), [^{11}C]6Me*m*Tyr for DAS (B), and [^{11}C]Raclopride for D_2R (C) clearly imaged the striatum of the normal monkey brain. After the repeated treatment with MPTP, presynaptic DAT availability assessed using [^{11}C]PE2I was significantly lower in the caudate (4.0% of normal), putamen (4.9% of normal), and SNc (18.6% of normal) (E) of the MPTP-treated monkey brain than in the normal monkey (A). Another presynaptic parameter of DAS assessed using [^{11}C]6Me*m*Tyr was also markedly lower in the caudate (13.6% of normal), putamen (12.3% of normal), and SNc (41.1% of normal) (F) of MPTP monkey brain than in normal animal monkey brain (B). In contrast, no significant changes in [^{11}C]Raclopride binding to postsynaptic D_2R were observed in the striatum or SNc between normal (C) and MPTP-treated animals (G).

The effects of the MPTP treatments on PET images of MC-I in the brain are shown in **Figure 5D** and **H**. The cerebral uptake of [^{18}F]BCPP-EF in normal monkeys showed homogeneous and symmetric patterns in the both hemispheres with clear separation of the cortical and basal ganglion regions (D). After the repeated treatment with MPTP, the V_T of [^{18}F]BCPP-EF exhibited significant reductions ranging between 60 and 70% of normal levels not only in the nigrostriatal pathway with abundant DA neurons but also in extra-striatal non-DA regions such as the cortex (H). No significant decreases in the V_T of [^{18}F]BCPP-EF were observed in the cerebellum.

Since the chronic treatment with MPTP, known as a DA specific toxin, unexpectedly induced decreases in MC-I activity in extra-striatal non-DA regions, another monoaminergic neuronal system of 5-HT was further evaluated. In the normal monkey brain, [^{11}C]DASB binding to SERT was high in the striatal and midbrain regions (**Figure 6A**), while [^{18}F]MPPF binding to 5-HT_{1A}R was high in the cortical regions (B). The quantitative analysis of [^{11}C]DASB revealed significantly lower SERT availability throughout the brain in MPTP-treated monkey, except the raphe nucleus (**Figure 6C**), than in normal monkeys (A). The reduction in [^{11}C]DASB availability to SERT was the greatest in the occipital cortex (19.7% of normal); intermediate in the frontal, parietal, and temporal cortices (50.0, 40.7, and 51.6% of normal); smaller in the caudate (60.3% of normal); and the smallest in the putamen and SNc (66.0 and 67.7% of normal). In contrast, no significant changes were observed in [^{18}F]MPPF binding to 5-HT_{1A}R throughout the brain between normal (**Figure 3B**) and MPTP-treated monkeys (D).

In order to assess the relationship between MC-I and DA and 5-HT neuronal systems in MPTP-treated monkey brains, the degrees of reductions in DAT measured using [^{11}C]PE2I, DAS measured using [^{11}C]6Me*m*Tyr in the nigrostriatal pathway (caudate, putamen, and SNc), and SERT measured using [^{11}C]DASB in

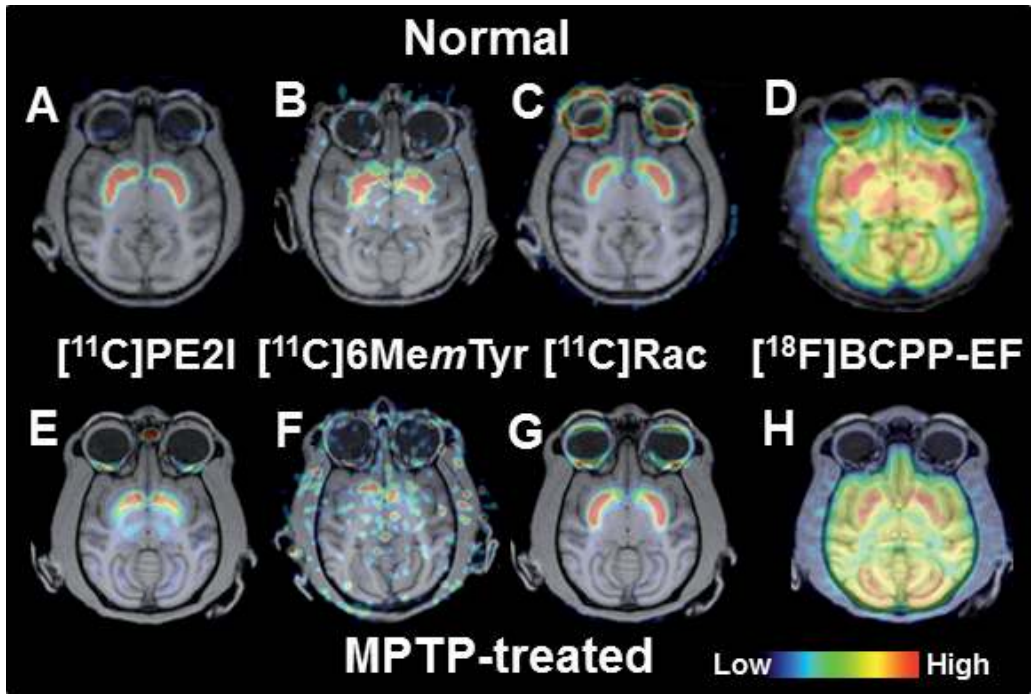

Figure 5.
*Effects of the MPTP treatment on PET images of DA and MC-I in living brains of conscious monkeys. PET scans were conducted for 91 min using [^{11}C]PE2I for DAT (A and E) and [^{18}F]BCPP-EF for MC-I (D and H) and for 60 min using [^{11}C]6Me*m*Tyr for DAS (B and F) and [^{11}C]Raclopride for D_2R (C and D). V_T images of [^{18}F]BCPP-EF (D and H) were created using a Logan graphical plot analysis with metabolite-corrected plasma input. BP_{ND} images of [^{11}C]PE2I (A and E) and ^{11}C-Raclopride (C and G) and multiple-time graphical analysis Ki images of [^{11}C]6Me*m*Tyr (B and F) were created using the corresponding TACs in the cerebellum as input functions.*

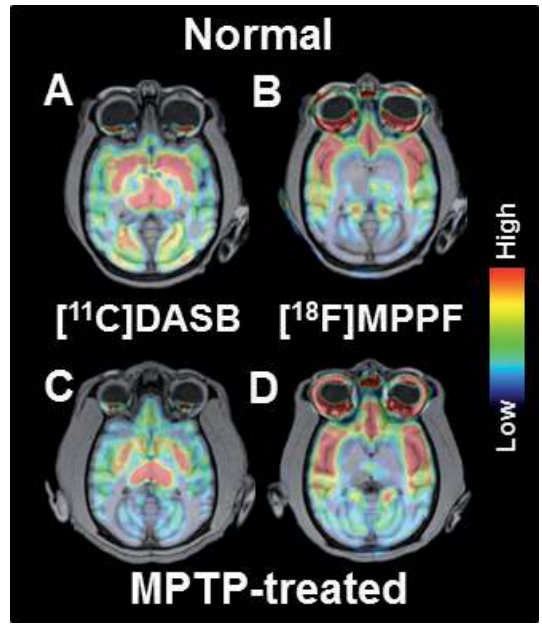

Figure 6.
Effects of the MPTP treatment on PET images of 5-HT in living brains of conscious monkeys. PET scans were conducted for 91 min with [^{11}C]DASB for SERT (A and C) and [^{18}FMPPF for 5-$HT_{1A}R$ (B and D). BP_{ND} images of [^{11}C]DASB (A and C) and [^{18}F]MPPF (B and D) were created using the corresponding TACs in the cerebellum as input functions.

the nigrostriatal and cortical (frontal, occipital, temporal, and parietal cortices) regions were plotted against those in MC-I measured using [^{18}F]BCPP-EF. Positive correlations were observed between the ΔBP_{ND} of [^{11}C]PE2I and ΔV_T of [^{18}F] BCPP-EF and between ΔKi of [^{11}C]6Me*m*Tyr and ΔV_T of [^{18}F]BCPP-EF in the nigrostriatal regions. In addition to the DA system, a positive correlation was noted between the ΔBP_{ND} of [^{11}C]DASB and ΔV_T of [^{18}F]BCPP-EF in the cortical regions, while no correlation was found between ΔBP_{ND} of [^{11}C]DASB and ΔV_T of [^{18}F] BCPP-EF in the nigrostriatal regions.

4.3 Discussion

The administration of MPTP causes the slow progressive loss of DA neurons over a period of several months, and the decrease in nigrostriatal DA levels is responsible for the motor symptoms of MPTP-treated animals, resembling clinical symptoms in PD patient. Thus, impaired ETC for OXPHOS due to a MC-I deficiency may account for neuronal cell death in PD. Alternatively, the MC-I deficiency in nigrostriatal DA system of PD patients may be secondary to mitochondrial damage due to oxidative stress. MC-I is a site of ROS production and is particularly vulnerable to oxidative damage [57]. The results of the present study showing a deficiency in presynaptic DA activity in the nigrostriatal pathway were consistent with the conventional theory shown above.

In contrast, the present study applying [^{18}F]BCPP-EF, a novel PET probe for MC-I, demonstrated that systemic and chronic MPTP treatments induced neuronal damage not only in the nigrostriatal DA pathway but also in the 5-HT neuronal system in the cortex of the monkey brain. Recent clinical studies suggested that in addition to motor symptoms, which are exclusively related to the nigrostriatal DA system, PD is a disease associated with non-motor symptoms, such as depression and cognitive deficits, which may be related to changes in other monoamines (noradrenaline and serotonin) in extra-striatal regions [58]. Lewy body and neurite deposition, a pathological hallmark of PD, occurs within the raphe nucleus containing 5-HT neurons of the caudal brainstem [59]. Decreases in 5-HT concentrations have been reported in the cortical regions of the postmortem brains of PD patients [60]. Furthermore, PET imaging on non-depressed PD patients revealed diffuse reductions in SERT availability throughout the brain [61] and decreased 5-HT_{1A}R binding in the brains of non-depressed and depressed PD patients [62]. The present results obtained in MPTP-treated monkeys were consistent with the recent clinical observations on 5-HT abnormalities in PD patients, which cannot be diagnosed by PET measurements of dopaminergic parameters only.

5. Conclusion

This chapter introduced the potential of [^{18}F]BCPP-EF as a PET probe for the noninvasive and quantitative imaging of MC-I activity in the living brain. The detectability of MC-I impairments using [^{18}F]BCPP-EF for neuronal damage in AD appears to be superior to the assessment of glucose metabolism measured using conventional [^{18}F]FDG. Furthermore, impaired serotonergic neuronal function in cortical regions suggests a relationship with depressive syndrome in PD patients. PET imaging of mitochondria function using [^{18}F]BCPP-EF will provide novel insights into the pathology, diagnosis, and treatment efficacy assessments of a wide range of neurodegenerative diseases, including AD, PD, HD, ALS, and MS.

Acknowledgements

We gratefully acknowledge the technical assistant of the members of the PET research group of Central Research Laboratory, Hamamatsu Photonics for PET studies.

Conflict of interest

All authors are employees of Hamamatsu Photonics K.K., and this research was supported by the company's budget. The authors declare that they have no competing interests.

Author details

Hideo Tsukada
Central Research Laboratory, Hamamatsu Photonics K.K., Hamamatsu, Shizuoka, Japan

*Address all correspondence to: tsukada@crl.hpk.co.jp

References

[1] Bolanos JP, Almeida A, Moncada S. Glycolysis: A bioenergetic or a survival pathway? Trends in Biochemical Sciences. 2010;**35**:145-149. DOI: 10.1016/j.tibs.2009.10.006

[2] Lopez-Otin C, Blasco MA, Partridge L, Serrano M, Kroemer G. The hallmarks of aging. Cell. 2013;**153**:1194-1217. DOI: 10.1016/j.cell.2013.05.039

[3] Spires-Jones TL, Hyman BT. The intersection of amyloid beta and tau at synapses in Alzheimer's disease. Neuron. 2014;**82**:756-771. DOI: 10.1016/j.neuron.2014.05.004

[4] Spillantini MG, Schmidt ML, Lee VM, Trojanowski JQ, Jakes R, Goedert M. Alpha-synuclein in Lewy bodies. Nature. 1997;**388**:839-840. DOI: 10.1038/42166

[5] Schapira AHV, Cooper JM, Dexter D, Clark JB, Jenner P, Marsden CD. Mitochondrial complex I deficiency in Parkinson's disease. Journal of Neurochemistry. 1990;**54**:823-827. DOI: 10.1111/j.1471-4159.1990.tb02325.x

[6] Keeney PM, Xie J, Capaldi RA, Bennett JP Jr. Parkinson's disease brain mitochondrial complex I has oxidatively damaged subunits and is functionally impaired and misassembled. The Journal of Neuroscience. 2006;**26**:5256-5264. DOI: 10.1523/JNEUROSCI.0984-06.2006

[7] Tsukada H. The use of ^{18}F-BCPP-EF as a PET probe for complex I activity in the Brain. In: Murphy AN, Chan DC, editors. Methods in Enzymology. Vol. 547. Burlington: Academic Press; 2014. pp. 417-431. DOI: 10.1016/B978-0-12-801415-8.00020-5

[8] Navarro A, Boveris A. Rat brain and liver mitochondria develop oxidative stress and lose enzymatic activities on aging. American Journal of Physiology. Regulatory, Integrative and Comparative Physiology. 2004;**287**:R1244-R1249. DOI: 10.1152/ajpregu.00226.2004

[9] Stauch KL, Purnell PR, Fox HS. Quantitative proteomics of synaptic and nonsynaptic mitochondria: Insights for synaptic mitochondrial vulnerability. Journal of Proteome Research. 2014;**13**:2620-2636. DOI: 10.1021/pr500295n

[10] Nabulsi NB, Mercier J, Holden D, Carré S, Najafzadeh S, Vandergeten M-C, et al. Synthesis and preclinical evaluation of ^{11}C-UCB-J as a PET tracer for imaging the synaptic vesicle glycoprotein 2A in the brain. Journal of Nuclear Medicine. 2016;**57**:777-784. DOI: 10.2967/jnumed.115.168179

[11] Tsukada H, Ohba H, Kanazawa M, Kakiuchi T, Harada N. Evaluation of ^{18}F-BCPP-EF for mitochondrial complex I imaging in conscious monkey brain using PET. European Journal of Nuclear Medicine and Molecular Imaging. 2014;**41**:755-763. DOI: 10.1007/s00259-013-2628-z

[12] Tsukada H, Nishiyama S, Ohba H, Kanazawa M, Kakiuchi T, Harada N. Comparing amyloid-β deposition, neuroinflammation, glucose metabolism, and mitochondrial complex I activity in brain: A PET Study in aged monkeys. European Journal of Nuclear Medicine and Molecular Imaging. 2014;**41**:2127-2136. DOI: 10.1007/s00259-014-2821-8

[13] Kanazawa M, Ohba H, Nishiyama S, Kakiuchi T, Tsukada H. Effects of MPTP on serotonergic neuronal systems and mitochondrial complex I activity in the living brain: A PET study on conscious rhesus monkeys. Journal of Nuclear Medicine. 2017;**58**:1111-1116. DOI: 10.2967/jnumed.116.189159

[14] Hashimoto F, Ohba H, Kanazawa M, Nishiyama S, Kakiuchi T, Tsukada H. Mitochondrial complex I deficit in the olfactory systems of age-related neurodegenerative monkey models: A PET study using ^{18}F-BCPP-EF. Journal of Alzheimers Disease and Parkinsonism. 2018;**8**:433. DOI: 10.4172/2161-0460.1000433

[15] Tsukada H, Nishiyama S, Fukumoto D, Kanazawa M, Harada N. Novel PET probes ^{18}F-BCPP-EF and ^{18}F-BCPP-BF for mitochondrial complex I: A PET study by comparison with ^{18}F-BMS-747158-02 in rat brain. Journal of Nuclear Medicine. 2014;**55**:473-480. DOI: 10.2967/jnumed.113.125328

[16] Tanaka E, Kudo H. Optimal relaxation parameters of DRAMA (dynamic RAMLA) aiming at one-pass image reconstruction for 3D-PET. Physics in Medicine and Biology. 2010;**55**:2917-2939. DOI: 10.1088/0031-9155/55/10/009

[17] Logan J, Fowler JS, Volkow ND, Wang GJ, Ding YS, Alexoff DL. Distribution volume ratios without blood sampling from graphical analysis of P'ET data. Journal of Cerebral Blood Flow and Metabolism. 1996;**16**:834-840. DOI: 10.1097/00004647-199609000-00008

[18] Yalamanchili P, Wexler E, Hayes M, Yu M, Bozek J, Kagan M, et al. Mechanism of uptake and retention of F-18 BMS-747158-02 in cardiomyocytes: A novel PET myocardial imaging agent. Journal of Nuclear Cardiology. 2007;**14**:782-788. DOI: 10.1016/j.nuclcard.2007.07.009

[19] Tsukada H, Ohba H, Nishiyama S, Kanazawa M, Kakiuchi T, Harada N. PET imaging of ischemia-induced impairment of mitochondrial complex I function in monkey brain. Journal of Cerebral Blood Flow and Metabolism. 2014;**34**:708-714. DOI: 10.1038/jcbfm.2014.5

[20] Ojaimi J, Masters CL, Opeskin K, McKelvie P, Byrne E. Mitochondrial respiratory chain activity in the human brain as a function of age. Mechanisms of Ageing and Development. 1999;**111**:39-47. DOI: 10.1016/S0047-6374(99)00071-8

[21] Navarro A, Boveris A. The mitochondrial energy transduction system and the aging process. American Journal of Physiology. Cell Physiology. 2007;**292**:C670-C686

[22] Manczak M, Jung Y, Park BS, Partovi D, Reddy PH. Time-course of mitochondrial gene expressions in mice brains: Implications for mitochondrial dysfunction, oxidative damage, and cytochrome c in aging. Journal of Neurochemistry. 2005;**92**:494-504. DOI: 10.1111/j.1471-4159.2004.02884.x

[23] Nakamura H, Kobayashi S, Ohashi Y, Anso S. Age-changes of brain synapses and synaptic plasticity in response to an enriched environment. Journal of Neuroscience Research. 1999;**56**:307-315. DOI: 10.1002/(SICI)1097-4547(19990501)56:3<307::AID-JNR10>3.0.CO;2-3

[24] Mostany R, Anstey JE, Crump KL, Maco B, Knott G, Portera-Cailliau C. Altered synaptic dynamics during normal brain aging. The Journal of Neuroscience. 2013;**33**:4094-4104. DOI: 10.1523/JNEUROSCI.4825-12.2013

[25] Li Z, Okamoto K, Hayashi Y, Sheng M. The Importance of dendritic mitochondria in the morphogenesis and plasticity of spines and synapses. Cell. 2004;**119**:873-887. DOI: 10.1016/j.cell.2004.11.003

[26] Cao L, Schrank BR, Rodriguez S, Benz EG, Moulia TW, Rickenbacher GT, et al. Aβ alters the connectivity of olfactory neurons in the absence of amyloid plaques in vivo. Nature Communications. 2012;**3**:1009. DOI: 10.1038/ncomms2013

[27] Allsop D, Mayes J, Moore S, Masad A, Tabner BJ. Metal-dependent generation of reactive oxygen species from amyloid proteins implicated in neurodegenerative disease. Biochemical Society Transactions. 2008;**36**:1293-1298. DOI: 10.1042/BST0361293

[28] Ingelsson M, Fukumoto H, Newell KL, Growdon JH, Hedley-Whyte ET, Frosch MP, et al. Early Aβ accumulation and progressive synaptic loss, gliosis, and tangle formation in AD brain. Neurology. 2004;**62**:925-931. DOI: 10.1212/01.WNL.0000115115.98960.37

[29] Monson NL, Ireland SJ, Ligocki AJ, Chen D, Rounds WH, Li M, et al. Elevated CNS inflammation in patients with preclinical Alzheimer's disease. Journal of Cerebral Blood Flow and Metabolism. 2014;**34**:30-33. DOI: 10.1038/jcbfm.2013.183

[30] Klunk WE, Engler H, Nordberg A, Wang Y, Blomqvist G, Holt DP, et al. Imaging brain amyloid in Alzheimer's disease with Pittsburgh Compound-B. Annals of Neurology. 2004;**55**:306-319. DOI: 10.1002/ana.2009

[31] Boutin H, Chauveau F, Thominiaux C, Gregoire MC, James ML, Trebossen R, et al. Receptor PET ligand for in vivo imaging of neuroinflammation. Journal of Nuclear Medicine. 2007;**48**:573-581. DOI: 10.2967/jnumed.106.036764

[32] Price JC, Klunk WE, Lopresti BJ, Lu X, Hoge JA, Ziolko SK, et al. Kinetic modeling of amyloid binding in humans using PET imaging and Pittsburgh compound-B. Journal of Cerebral Blood Flow and Metabolism. 2005;**25**:1528-1547. DOI: 10.1038/sj.jcbfm.9600146

[33] Kumar A, Muzik O, Shandal V, Chugani D, Chakraborty P, Chugani HT. Evaluation of age-related changes in translocator protein (TSPO) in human brain using ^{11}C-[R]-PK11195 PET. Journal of Neuroinflammation. 2012;**9**:232. DOI: 10.1186/1742-2094-9-232

[34] Dukart J, Mueller K, Horstmann A, Vogt B, Frisch S, Barthel H, et al. Differential effects of global and cerebellar normalization on detection and differentiation of dementia in FDG-PET studies. NeuroImage. 2010;**49**:1490-1495. DOI: 10.1016/j.neuroimage.2009.09.017

[35] Finch CE, Austad SN. Primate aging in the mammalian scheme: The puzzle of extreme variation in brain aging. Age. 2012;**34**:1075-1091. DOI: 10.1007/s11357-011-9355-9

[36] Noda A, Murakami Y, Nishiyama S, Fukumoto D, Miyoshi S, Tsukada H, et al. Amyloid imaging in aged and young macaques with [^{11}C]PIB and [^{18}F]FDDNP. Synapse. 2008;**62**:472-475. DOI: 10.1002/syn.20508

[37] Edison P, Archer HA, Hinz R, Hammers A, Pavese N, Tai YF, et al. Amyloid, hypometabolism, and cognition in Alzheimer disease: An [^{11}C]PIB and [^{18}F]FDG PET study. Neurology. 2007;**68**:501-508. DOI: 10.1212/01.wnl.0000244749.20056.d4

[38] Kemppainen NM, Aalto S, Wilson LA, Nagren K, Helin S, Bruck A, et al. PET amyloid ligand [^{11}C]PIB uptake is increased in mild cognitive impairment. Neurology. 2007;**68**:1603-1606. DOI: 10.1212/01.wnl.0000260969.94695.56

[39] Swomley AM, Förster S, Keeney JT, Triplett J, Zhang Z, Sultana R, et al. Aβ, oxidative stress in Alzheimer disease: Evidence based on proteomics studies. Biochimica et Biophysica Acta. 2014;**1842**:1248-1257

[40] Schon EA, Przedborski S. Mitochondria: The next (neurode) generation. Neuron. 2011;**70**:1033-1053. DOI: 10.1016/j.neuron.2011.06.003

[41] Lin MT, Beal MF. Mitochondrial dysfunction and oxidative stress in neurodegenerative diseases. Nature. 2006;**443**:787-795. DOI: 10.1038/nature05292

[42] Pagani L, Eckert A. Amyloid-beta interaction with mitochondria. International Journal of Alzheimer's Disease. 2011;**2011**:1-12. DOI: 10.4061/2011/925050

[43] Kish SJ, Shannak K, Hornykiewicz O. Uneven pattern of dopamine loss in the striatum of patients with idiopathic Parkinson's disease. Pathophysiologic and clinical implications. The New England Journal of Medicine. 1988;**318**:876-880. DOI: 10.1056/NEJM198804073181402

[44] Recasens A, Dehay B, Bove J, Carballo-Carbajal I, Dovero S, Perez-Villalba A, et al. Lewy body extracts from Parkinson disease brains trigger alpha-synuclein pathology and neurodegeneration in mice and monkeys. Annals of Neurology. 2014;**75**:351-362. DOI: 10.1002/ana.24066

[45] Shimozawa A, Ono M, Takahara D, Tarutani A, Imura S, Masuda-Suzukake M, et al. Propagation of pathological α-synuclein in marmoset brain. Acta Neuropathologica Communications. 2017;**5**:12. DOI: 10.1186/s40478-017-0413-0

[46] Ludtmann MHR, Angelova PR, Horrocks MH, Choi ML, Rodrigues M, Baev AY, et al. α-Synuclein oligomers interact with ATP synthase and open the permeability transition pore in Parkinson's disease. Nature Communications. 2018;**9**:2293. DOI: 10.1038/s41467-018-04422-2

[47] Burns RS, Chiueh CC, Markey SP, Ebert MH, Jacobowitz DM, Kopin IJ. A primate model of parkinsonism: Selective destruction of dopaminergic neurons in the pars compacts of the substantia nigra by MPTP. Proceedings of the National Academy of Sciences of the United States of America. 1983;**80**:4546-4550. DOI: 10.1073/pnas.80.14.4546

[48] Muramatsu S, Okuno T, Suzuki Y, Nakayama T, Kakiuchi T, Takino N, et al. Multitracer assessment of dopamine function after transplantation of embryonic stem cell-derived neural stem cells in a primate model of Parkinson's disease. Synapse. 2009;**63**:541-548. DOI: 10.1002/syn.20634

[49] Tsukada H, Kanazawa M, Ohba H, Nishiyama S, Harada N, Kakiuchi T. PET imaging of mitochondrial complex I with ^{18}F-BCPP-EF in brain of Parkinson's disease model monkey. Journal of Nuclear Medicine. 2016;**57**:950-953. DOI: 10.2967/jnumed.115.169615

[50] Wilson AA, Ginovart N, Schmidt M, Meyer JH, Threlkeld PG, Houle S. Novel radiotracers for imaging the serotonin transporter by positron emission tomography: Synthesis, radiosynthesis, and in vitro and ex vivo evaluation of ^{11}C-labeled 2-(phenylthio) araalkylamines. Journal of Medicinal Chemistry. 2000;**43**:3103-3110. DOI: 10.1021/jm000079i

[51] Le Bars D, Lemaire C, Ginovart N, et al. High-yield radiosynthesis and preliminary in vivo evaluation of p-[^{18}F]MPPF, a fluoro analog of WAY-100635. Nuclear Medicine and Biology. 1998;**25**:343-350. DOI: 10.1016/S0969-8051(97)00229-1

[52] Kanazawa M, Ohba H, Iwazaki A, Kakiuchi T, Tsukada H. Synthesis of 6-^{11}C-methyl-*m*-tyrosine (^{11}C-6Me*m*Tyr) for dopamine synthesis imaging in living brain using PET. Bioorganic and Medicinal Chemistry. 2015;**23**:729-734. DOI: 10.1016/j.bmc.2014.12.061

[53] Kanazawa M, Ohba H, Harada N, Kakiuchi T, Muramatsu S, Tsukada H. Evaluation of 6-^{11}C-methyl-*m*-tyrosine as a PET probe for presynaptic dopaminergic activity: A comparison PET study with β-^{11}C-L-DOPA and ^{18}F-FDOPA in Parkinson's disease monkeys. Journal of Nuclear Medicine. 2016;**57**:303-308. DOI: 10.2967/jnumed.115.161802

[54] Halldin C, Erixon-Lindroth N, Pauli S, Chou YH, Okubo Y, Karlsson P, et al. [^{11}C]PE2I: A highly selective radioligand for PET examination of the dopamine transporter in monkey and human brain. The European Journal of Nuclear Medicine and Molecular Imaging. 2003;**30**:1220-1230. DOI: 10.1007/s00259-003-1212-3

[55] Innis RB, Cunningham VJ, Delforge J, Fujita M, Gjedde A, Gunn RN, et al. Consensus nomenclature for in vivo imaging of reversibly binding radioligands. Journal of Cerebral Blood Flow and Metabolism. 2007;**27**:1533-1539. DOI: 10.1038/sj.jcbfm.9600493

[56] Patlak CS, Blasberg RG. Graphical evaluation of blood-to-brain transfer constants from multiple-time uptake data: Generalizations. Journal of Cerebral Blood Flow and Metabolism. 1985;**5**:584-590. DOI: 10.1038/jcbfm.1985.87

[57] Robinson BH. Human complex I deficiency: Clinical spectrum and involvement of oxygen free radicals in the pathogenicity of the defect. Biochimica et Biophysica Acta. 1998;**1364**:271-286. DOI: 10.1016/S0005-2728(98)00033-4

[58] Chaudhuri KR, Healy DG, Schapira AH. Non-motor symptoms of Parkinson's disease: Diagnosis and management. Lancet Neurology. 2006;**5**:235-245. DOI: 10.1016/S1474-4422(06)70373-8

[59] Orth M, Schapira AHV. Mitochondrial involvement in Parkinson's disease. Neurochemistry International. 2002;**40**:533-541. DOI: 10.1016/S0197-0186(01)00124-3

[60] Scatton B, Javoy-Agid F, Rouquier L, Dubois B, Agid Y. Reduction of cortical dopamine, noradrenaline, serotonin and their metabolites in Parkinson's disease. Brain Research. 1998;**275**:321-328. DOI: 10.1016/0006-8993(83)90993-9

[61] Albin RL, Koeppe RA, Bohnen NI, Wernette K, Kilbourn MA, Frey KA. Spared caudal brainstem SERT binding in early Parkinson's disease. Journal of Cerebral Blood Flow and Metabolism. 2008;**28**:441-444. DOI: 10.1038/sj.jcbfm.9600599

[62] Ballanger B, Klinger H, Eche J, Lerond J, Vallet AE, Le Bars D, et al. Role of serotonergic 1A receptor dysfunction in depression associated with Parkinson's disease. Movement Disorders. 2012;**27**:84-89. DOI: 10.1002/mds.23895